Computer Fraud and Security
ISSN (online): 1873-7056

Insulator Overheating Infrared Image Detection Method Based on Improved YOLOv8

Hongrun Feng*, Jining Zhao, Zihao Liu, Yanhui Meng, Rong Meng, Xiaodan Fan
Ultra High Voltage Branch, State Grid Hebei Electric Power Co., Ltd., Shijiazhuang, China
**Corresponding Author's Email: fenghongrundq@163.com*

Abstract: Insulators are an important part of transmission lines, insulator deterioration, failure and other problems are one of the main causes of transmission line failure, and insulator deterioration, failure is often accompanied by insulators appear abnormal temperature rise, so there is a need to carry out a rapid assessment of the insulator heating condition, and can be monitored in real time at the edge end of the algorithmic approach. In this paper, to address the above problems, the improved YOLOv8 algorithm is used to improve the YOLOv8 algorithm for the insulator infrared image of the overheating region of the target recognition approach. Firstly, the YOLOv8 target detection algorithm is improved by introducing the CBAM attention mechanism, i.e., by introducing the channel and spatial attention module in the CNN (Convolutional Neural Network) to improve the perceptual ability of the overall model and improve the performance without increasing the network complexity. Then the deformable convolution DCNv3 is introduced to generate learnable offsets to improve the traditional fixed convolution operation, which realizes nonlinear sampling of the input feature maps during the convolution process and improves the robustness and accuracy of the algorithm. Finally, the WioU loss function is introduced to optimize the network, which is experimentally verified to achieve an inference accuracy of 87.5% mAP at the edge end of the device to meet the identification of abnormal temperature rise of insulators at the edge end, and the comparative test proves the effectiveness and superiority of the algorithm proposed in this paper through ablation.

Keywords: Infrared image; Temperature rise assessment; Target recognition; YOLOv8

1. Introduction

In China's high-voltage AC transmission lines, insulators serve the critical function of providing electrical insulation and structural support, making their operational safety paramount to power grid reliability. However, during routine grid operations, porcelain insulators are prone to develop microscopic air bubbles and hairline cracks. These defects progressively expand with prolonged service, adversely impacting the insulation performance by reducing resistance values. Furthermore, the electromagnetic fields in high-voltage lines and the mechanical stress sustained by insulators collectively contribute to the degradation of insulation performance, resulting in continuous resistance reduction. Ultimately, when an insulator's resistance diminishes to critical thresholds—manifesting as low-resistance or zero-resistance insulators—it poses substantial risks to transmission line safety [1-5].

In current practice for detecting insulator degradation and failures, manual tower-climbing inspection remains a widely adopted approach. This method primarily employs the following techniques: voltage distribution measurement, impulse current detection, spark gap testing, electric field evaluation, and leakage current monitoring to identify low-resistance or zero-resistance insulators. However, these conventional methods present significant operational limitations, including poor temporal resolution, high labor costs, inherent safety hazards that are difficult to mitigate, and suboptimal efficiency. To address these challenges while enhancing worker safety, reducing operational expenses, and achieving rapid detection, infrared thermographic analysis of insulators has emerged as a viable technical solution.

Low-resistance and zero-resistance insulators exhibit distinct thermal characteristics due to their reduced resistance and compromised insulation performance, while insulator faults also induce abnormal temperature rises. Leveraging this thermal behavior for detection—specifically through monitoring anomalous temperature

elevations—enables efficient early warning and assessment of insulator anomalies, thereby enhancing grid operational safety. This inherent advantage has driven increasing adoption of infrared thermography [6-11].

Recent years have witnessed progressive advancements in infrared thermal image recognition research. Duan Zhongxing et al. [12] addressed critical challenges in power equipment infrared imaging, including data imbalance and variability, by implementing multi-scale convolutional modules within the YOLOv4 backbone network and employing Focal Loss to enhance initial feature representation, effectively resolving classification difficulties caused by imbalanced infrared datasets. Gu Xing et al. [13] improved feature extraction through attention mechanisms and optimized iterative feature pyramid structures, achieving superior multi-scale target recognition. Their integration of CIoU loss functions with Gradient Harmonized Mechanisms significantly enhanced detection accuracy and processing speed. Zhou Yangyang et al. [14] incorporated dilated convolution kernels into depthwise separable convolutions, developing a D-MobileNet architecture to replace the ELANCSP backbone in YOLOv7, resulting in improved robustness, generalization capability, and model lightweighting. Liu Guote et al. [15] proposed an AI-driven recognition method using enhanced cascaded Gentle Adaboost classifiers for post insulator infrared images, establishing an efficient framework for multi-target fault diagnosis and identification. Wang Yuanbin et al. [16] implemented a YOLOv5-based infrared recognition system featuring Ghost convolutions in the backbone network, channel interaction-enhanced attention modules, and self-attention-optimized C3 modules. Their integration of Cluster NMS and EIoU loss functions accelerated network convergence while maintaining precision.

Current infrared detection methods for insulator overheating caused by degradation or faults rely primarily on thermal signature analysis. However, practical challenges persist due to the variable geometries, inconsistent scales, and complex backgrounds of overheated insulators in infrared images, which impair effective feature extraction and consequently limit detection accuracy. To enhance recognition performance for overheated porcelain insulators under degradation/fault conditions, this study proposes an improved YOLOv8-based infrared target detection method, with potential for expansion into insulator fault warning platforms.

Our modifications to the baseline YOLOv8 architecture include: 1) Integration of the CBAM attention mechanism [17] to enhance feature discrimination without increasing computational complexity; 2) Implementation of deformable convolution DCNv3 [18], which introduces learnable offset parameters to replace conventional fixed convolution kernels, enabling nonlinear sampling of input features and improved detection accuracy for irregularly shaped insulators; 3) Adoption of WIoU loss [19] to optimize bounding box regression, particularly enhancing precision when detecting multiple insulator components. These innovations collectively improve adaptation to actual transmission line conditions while maintaining detection efficiency.

2. Insulator Target Detection Method Based on Improved YOLOv8 Algorithm

2.1 Insulator Heating Mechanism

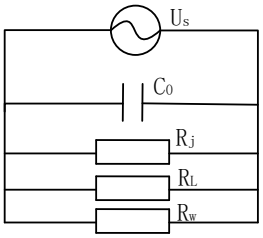

Figure. 1 Degraded insulator equivalent circuit diagram

Over time, contaminant deposition, surface degradation, and declining mechanical properties on insulator surfaces collectively impair insulation performance through resistance reduction. Both surface leakage currents and internal penetrating leakage currents significantly influence insulator heating characteristics [20].

The equivalent circuit of degraded insulators is illustrated in Figure 1, where C_0 represents inter-electrode capacitance, while Rj , R_L , and R_W denote equivalent resistances for polarization loss heating, primary

insulation degradation pathways, and leakage loss respectively. The thermal power generation is expressed in Equation (1):

$$P = (\frac{Z_S U_N}{Z_S + Z_D}) \times (\frac{1}{R_j} + \frac{1}{R_L}) \quad (1)$$

In Equation (1), Z_D corresponds to the equivalent impedance across the insulator string, and Zs represents the inter-electrode equivalent impedance, calculated through Equation (2):

$$Z_s = \frac{R_L \cdot R_j}{R_j + R_L + R_j \cdot R_L \cdot j\omega C_0} \quad (2)$$

Infrared-based insulator detection fundamentally exploits these thermal generation mechanisms. Progressive operational aging induces microscopic air bubbles and hairline cracks within insulators, initiating material degradation that reduces insulation capacity and resistance. As deterioration intensifies, this process ultimately culminates in insulator overheating conditions.

2.2 Improved YOLOv8 Algorithm

Our methodology initiates with dataset construction using open-source and web-acquired infrared insulator images. Through multi-strategy data augmentation and meticulous annotation, we establish a comprehensive dataset containing insulators with thermal anomalies. Given YOLOv8's [21] demonstrated balance between detection accuracy and computational efficiency, we select it as the baseline model.

To address the complex background interference prevalent in transmission line environments, we integrate the CBAM (Convolutional Block Attention Module) [17], which synergistically combines channel attention and spatial attention mechanisms. Channel attention optimizes feature representation across different spectral bands, while spatial attention prioritizes critical positional information, collectively enhancing feature discriminability without increasing network complexity.

Furthermore, we implement deformable convolution DCNv3 [18] to replace conventional convolution operations. This innovation introduces learnable offset parameters that enable adaptive sampling of input feature maps, significantly improving detection precision for irregularly shaped insulators and enhancing model adaptability to real-world grid conditions.

Finally, we adopt the WIoU (Wise Intersection over Union) loss function [19] to refine bounding box regression. This advanced metric provides more accurate similarity evaluation between predicted and ground-truth boxes, particularly improving multi-component detection accuracy when analyzing complex insulator assemblies.

Figure. 2 YOLOv8 architecture diagram

2.2 CBAM Attention-Based Mechanisms

In 2018, Sanghyun Woo et al. proposed CBAM (Convolutional Block Attention Module) [17], an attention mechanism designed to enhance convolutional neural network (CNN) performance. CBAM improves model perceptiveness by sequentially integrating channel and spatial attention modules into CNNs without increasing computational complexity. Channel attention optimizes inter-channel feature representation, while spatial attention prioritizes critical spatial information.

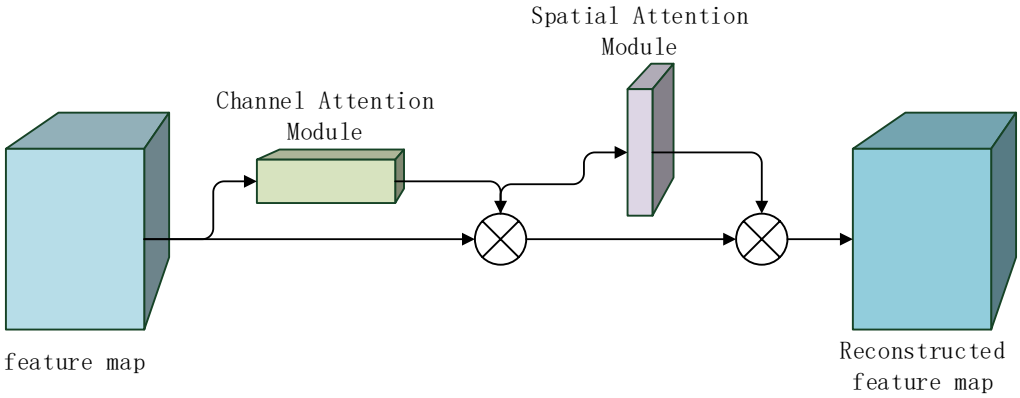

Figure. 3 CBAM architecture diagram

The CBAM mechanism generates attention-enhanced features through element-wise multiplication of channel and spatial attention outputs. These refined features propagate through subsequent network layers, preserving critical information while suppressing irrelevant features.

Figure. 4 Channel Attention Module

As shown in Figure 4, the channel attention mechanism processes input feature map F through parallel global max-pooling and global average-pooling operations along spatial dimensions (width × height). The resulting pooled features are fed into a shared two-layer MLP: the first layer contains C/r neurons with ReLU activation (where r denotes the reduction ratio), and the second layer contains C neurons. The MLP outputs are summed element-wise and activated via sigmoid to produce channel attention weights Mc. These weights are multiplied with input F to generate input features for the spatial attention module.

Figure. 5 Spatial Attention Module

Figure 5 illustrates the spatial attention workflow. The channel-refined feature F' undergoes concurrent global max-pooling and average-pooling across channel dimensions. The concatenated results are compressed to

single-channel features via 7×7 convolution, followed by sigmoid activation to produce spatial attention map Ms. Final output features are obtained through element-wise multiplication between Ms and F'.

Figure. 6 C2fC module

Integrating CBAM into YOLOv8's Neck layer enhances the network's capacity to autonomously prioritize salient features while suppressing redundancy. Specifically, we embed CBAM within the original C2f module of YOLOv8's Neck layer, forming an enhanced C2fC module (Figure 6). This adaptation strengthens feature extraction capabilities for insulator infrared images, which often suffer from complex background interference. By enabling selective focus on discriminative thermal patterns, the modified architecture improves recognition accuracy under cluttered transmission line conditions while maintaining computational efficiency.

2.3 Deformable Convolution DCNv3

Deformable Convolution (DCN) introduces learnable spatial transformations into convolutional neural networks by augmenting traditional fixed convolution operations with trainable offset parameters, enabling adaptive nonlinear sampling of input feature maps. DCNv3 [18], an enhanced iteration building upon DCNv1 and DCNv2, optimizes computational efficiency and feature adaptability, particularly enhancing model performance under constrained training data and limited training durations. Figure 7 illustrates the operational principle of deformable convolution.

Figure. 7 Deformable Convolution Schematic Diagram

For a standard 3×3 convolution kernel with 9 sampling points (Fig.7a), deformable convolution learns spatial offsets ( ) for each sampling position, dynamically adjusting kernel geometry to match target object morphologies.

In conventional 2D convolution, the output feature map y at position is computed as:

(3)

where R = {(-1, -1), (-1, 0), ..., (1, 1)} defines the regular sampling grid, and denotes convolution weights.

For DCNv3, the output is reformulated as:

(4)

where G represents the total aggregation groups. Each group maintains independent sampling offsets ( ) and modulation scalars ( ), enabling diverse spatial aggregation patterns. The convolution weights are decomposed into depth-wise (spatial filtering) and point-wise (channel projection) components. Modulation scalars , normalized via softmax along the k-dimension, regulate feature contributions. Input features are sliced per group, with denoting learned offsets for group g.

Figure. 8 The overall process of deformable convolution

Figure 8 details the implementation workflow: 1) A standard convolution generates offset fields (2N channels for x/y directional offsets); 2) Bilinear interpolation propagates offsets through differentiable sampling:

(5)

(6)

(7)

Here, q indexes input feature map positions, p denotes deformed sampling coordinates, and G(q,p) represents the bilinear interpolation kernel decomposed into 1D components.

Conventional convolution struggles with irregular insulator geometries, variable imaging perspectives, and cluttered backgrounds in infrared images, often causing feature loss. To address this, we replace standard convolutions in YOLOv8's SPPF module with DCNv3, creating an enhanced SPPFD module (Figure 9). This adaptation improves feature adaptability to complex infrared scenes while maintaining detection precision.

Figure. 9 SPPFD module structure

2.4 Wise-IoU Loss Function

The baseline YOLOv8 architecture employs DFL (Distribution Focal Loss) with CIoU (Complete Intersection over Union) as its loss function. While CIoU effectively measures bounding box overlap in most scenarios, it inadequately addresses training sets containing low-quality annotations by indiscriminately emphasizing regression accuracy for such samples, ultimately compromising detection robustness.

This study implements Wise-IoU (WIoU) to address these limitations. WIoU first calculates the fundamental IoU metric to quantify bounding box overlap, then applies minimum weighting coefficients to individual components of predicted and ground-truth boxes for precise contribution characterization. Finally, it normalizes the weighted IoU using maximum component weights. This weighting mechanism enables more accurate similarity assessment between detection outputs and targets, particularly enhancing multi-component object recognition accuracy. The WIoU formulation is defined as:

(8)

(9)

Where (x, y, w, h) denote the center coordinates, width, and height of predicted boxes; (xgt , ygt, wgt, hgt)represent corresponding ground-truth parameters; and specify the minimum enclosing box dimensions; and define intersection region measurements. The * operator indicates computational graph decoupling.

WIoU innovatively resolves CIoU's irrational aspect ratio integration through dual-layer distance-aware attention mechanisms. By establishing geometric-aware attention via distance metrics, it properly weights the impact of bounding box aspect ratios on loss computation. Furthermore, the decoupled treatment of minimum enclosing box dimensions mitigates excessive geometric penalties on low-quality samples, enabling better adaptation to annotation variability.

Implementation advantages include:

1.Reduced Training Intervention: Simplified hyperparameter tuning through self-adaptive weighting

2.Enhanced Generalization: Optimized loss formulation improves cross-scene adaptability

3.Geometric Robustness: Balanced consideration of distance and aspect ratio influences

4.Computational Efficiency: Maintained computational complexity comparable to CIoU

These improvements collectively enhance detection stability across diverse infrared insulator datasets while preserving real-time processing capabilities essential for grid monitoring applications.

3 Experiments and Analysis of Results

3.1 Insulator Infrared Image Dataset

Our dataset comprises infrared insulator images collected from open-source repositories, web resources, and real-world case libraries. Using LabelImg annotation tools, we meticulously labeled 2,668 images containing insulators with thermal anomalies, encompassing normal operational states, fault conditions, and challenging environmental scenarios including adverse weather and complex backgrounds to ensure comprehensive data diversity.

We implemented multi-modal data augmentation through geometric transformations: random rotation (±30°), horizontal/vertical flipping, scaling (0.5-1.5×), translation (±15% offset), and adaptive cropping. These operations expanded sample variability while preserving thermal signature integrity.

The processed dataset was partitioned into training and validation subsets at an 8:2 ratio, maintaining proportional representation of all anomaly categories. Both the baseline YOLOv8 implementation and our enhanced YOLOv8 architecture were trained on this standardized dataset under identical hardware configurations (NVIDIA RTX 3090 GPU, PyTorch 1.12 framework) to ensure comparative validity.

3.2 Comparative Experiments of Attentional Mechanisms

To compare and evaluate the effects and performance of different attention mechanisms in our proposed model, we utilize heat maps to reflect information about the network's focus locations, and conduct visual analysis through feature map visualization methods. In the generated heat maps, the varying color intensities across different regions indicate differences in regional weights, which represent each area's responsiveness to the overall network. Since this study primarily applies attention mechanisms to the feature enhancement module Neck layer to form C2fC modules, we specifically investigate the network's Neck layer. Figure 10 displays heat maps generated by the Neck layer under four configurations: original YOLOv8, Transformer attention mechanism, CA (Coordinate Attention) mechanism, and our adopted CBAM attention mechanism.

(a)YOLOv8 (b) Transformer Attention Mechanism

(c) CA attention mechanisms (d) CBAM Attention Mechanism

Figure. 10 Heatmaps of outputs from different network necks

Figure 10a shows the heat map from the original YOLOv8 Neck layer without any attention mechanisms, where the focus around overheated insulators is significantly insufficient, with dispersed attention distribution not concentrated on the insulators. Figures 10b and 10c present heat maps after implementing Transformer and CA attention mechanisms respectively, showing clearer attention concentration around overheated insulators, particularly more pronounced with CA mechanism. Figure 10d demonstrates the heat map using CBAM attention mechanism, displaying more focused attention precisely on the overheated insulator bodies compared to Figure 10c.

Figure. 10 Detection performance in real environments

To verify the practical applicability of our improved YOLOv8 algorithm under real-world conditions where infrared images often suffer from fog, strong winds, and imaging blur, we tested the algorithm with low-quality images from actual scenarios. Figure 11 shows partial detection results of overheated insulator infrared images, where "fault" labels indicate annotated defects. The detection outcomes demonstrate that our improved YOLOv8 algorithm maintains excellent detection performance under practical challenges like fog and wind interference, effectively identifying insulator overheating and confirming its real-world applicability.

3.3 Comparative Experiment

To evaluate the performance advantages of our improved YOLOv8 algorithm in inference accuracy and speed compared to other methods, we conducted comparative experiments using six algorithms: YOLO series variants (YOLOv5, YOLOv6, YOLOv7), Faster-RCNN, baseline YOLOv8, and our enhanced YOLOv8. All tests utilized identical thermal anomaly insulator infrared datasets and training hyperparameters. The comparative results are summarized in Table 1.

Table 1 Comparative experiment on improving YOLOv8 algorithm

Model	mAP@0.5/%	mAP@0.95/%	FPS	GFLOPs
YOLOv5	78.3	46.6	25	47.5
YOLOv6	80.7	47.5	17	84.3
YOLOv7	86.2	50.1	11	97.4
YOLOv8	86.0	49.8	23	27.2
Faster-RCNN	68.4	10.6	6	78.9
Improved Yolov8	87.5	51.8	22	27.4

As clearly demonstrated in Table 1, YOLOv5 achieves the highest inference speed at 25 fps while maintaining 78.3% accuracy, yet still shows significant accuracy gaps compared to our improved YOLOv8. Subsequent YOLO series iterations (YOLOv6 and YOLOv7) exhibit accuracy improvements over YOLOv5 at the cost of reduced inference speeds. Although YOLOv8 delivers comparable accuracy to YOLOv7, it achieves substantially faster inference speeds, justifying its selection as our baseline architecture. Faster-RCNN underperforms in both accuracy and speed metrics compared to YOLO-family algorithms.

Our enhanced YOLOv8 demonstrates superior performance—maintaining inference speeds equivalent to baseline YOLOv8 while achieving significant accuracy improvements. This optimized implementation outperforms all comparative methods in overall detection capability.

4. Conclusions

To address the requirement of target recognition in overheated insulator infrared images, this study proposes an enhanced network based on YOLOv8. Building upon the baseline YOLOv8 architecture, we integrate the CBAM attention mechanism , deformable convolution DCNv3 , and WIoU loss function to improve detection capabilities for thermally anomalous insulators. Experimental validation yields the following conclusions:

The proposed improved YOLOv8 algorithm achieves critical accuracy enhancements while maintaining comparable inference speed to the original implementation. Quantitative results demonstrate an increase in mAP@0.5 from 86.0% (baseline YOLOv8) to 87.5%, representing a 1.74% accuracy improvement, with inference speed decreasing marginally from 23 fps to 22 fps. Comparative experiments confirm our algorithm's superior overall performance against five alternative detection frameworks. This advancement enables high-precision edge-computing recognition of insulator thermal anomalies, providing technical foundations for developing insulator fault warning systems. The methodology demonstrates practical applicability in power grid condition monitoring applications.

Acknowledgements

The authors acknowledge the State Grid Hebei Electric Power Co.Ltd (Grant: kj2022-009).

Declaration of Conflicting Interests

The author(s) declared no potential conflicts of interest with respect to the research, author-ship, and/or publication of this article.

Data Sharing Agreement

The datasets used and/or analyzed during the current study are available from the corresponding author on reasonable request.

References

[1] S. Pei, H. Zhang, Y. Zhu et al. (2024) Lightweight transmission line defect identification method based on OFN network and distillation method, IET Image Process., 18 (12) :3518–3529.
[2] C. Hu, S. Pei, Y. Liu et al. (2023) Real-time defect detection method for transmission line edge end based on LEE-YOLOv7, High Volt. Eng., :1–14.
[3] H. Li, S. Guo, T. Xu et al. (2024) Transformer abnormal heat accurate identification method based on AHIPDNet, Sci. Rep., 14 (1) :29456.
[4] C. Hou, Z.L. Li, X.L. Shen et al. (2024) Real-time defect detection method based on YOLO-GSS at the edge end of a transmission line, IET Image Process., 18 (5) :1315–1327.
[5] Y. Zhou, Y.Z. Yan, H.Y. Chen et al. (2023) Defect detection of photovoltaic cells based on improved YOLOv8, Laser Optoelectron. Prog., 61 (8) :8–25.
[6] S. Pei, H. Zhang, Y. Liu et al. (2024) An efficient method to extract the axial temperature curve from infrared image of porcelain insulator string, IEEE Trans. Power Deliv.
[7] Y. Shao, R. Zhang, C. Lv et al. (2024) TL-YOLO: foreign-object detection on power transmission line based on improved YOLOv8, Electronics, 13 (8) :1543.
[8] Y. Yang, S. Yang, M. Yan et al. (2024) UDD-YOLO based edge-end insulator discharge severity assessment algorithm, J. Electron. Meas. Instrum., 38 (1) :219–227.
[9] L. Lin, Y. Wu (2024) Infrared overheating defect detection method for power equipment based on improved YOLOv7, Electr. Eng., 25 (1) :42–47.
[10] S. Kong, Z. Xu, X. Lin et al. (2023) Infrared thermal imaging defect detection of photovoltaic modules based on improved YOLO v5 algorithm, Infrared Technol., 45 (9) :974–981.
[11] W. Shen, Z. Song, S. Wang et al. (2023) Analysis of temperature rise characteristics of defective composite insulators based on infrared imaging, Nondestruct. Test., 45 (9) :5–11.
[12] Z. Duan, Y. Zhang, J. Ma (2022) Infrared image recognition of power equipment using improved YOLOv4, Laser Optoelectron. Prog., 59 (24) :29–36.
[13] X. Gu, W. Zhan, Z. Cui et al. (2023) Infrared target detection method based on attention mechanism, Laser Optoelectron. Prog., 60 (10) :293–300.
[14] Y. Zhou, J. Hu, H. Xu et al. (2023) An infrared image target detection algorithm for porcelain post insulators, Zhejiang Electr. Power, 42 (11) :78–85.
[15] G. Liu, W. Wu, F. Guo et al. (2022) AI recognition of post insulator infrared image based on improved cascade gentle Adaboost classifier, High Volt. Eng., 48 (3) :1088–1095.
[16] Y. Wang, Y. Li, Y. Duan et al. (2023) Infrared image recognition of substation equipment based on lightweight backbone network and attention mechanism, Power Syst. Technol., 47 (10) :4358–4369.
[17] S. Woo, J. Park, J.Y. Lee et al. (2018) CBAM: convolutional block attention module, Proc. Eur. Conf. Comput. Vis. (ECCV), :3–19.
[18] J.F. Dai, H.Z. Qi, Y.W. Xiong et al. (2017) Deformable convolutional networks, Proc. IEEE Int. Conf. Comput. Vis., :764–773.
[19] Z. Tong, Y. Chen, Z. Xu et al. (2023) Wise-IoU: bounding box regression loss with dynamic focusing mechanism, arXiv preprint arXiv:2301.10051.
[20] Z. Xia, L. Wang, J. Yang et al. (2020) Identification of degraded porcelain insulator in substation based on infrared thermal imaging technology, Guangdong Electr. Power, 33 (4) :105–111.
[21] R. Varghese, M. Sambath (2024) YOLOv8: a novel object detection algorithm with enhanced performance and robustness, Proc. Int. Conf. Adv. Data Eng. Intell. Comput. Syst., :1–6.